

# Experimental investigations on flapping flexible hawkmoth-like wings for insect-inspired flapping MAVs development

## 1 INTRODUCTION

In this paper, the hawkmoth hovering flight is investigated experimentally to support the development of Micro Aerial Vehicles (MAVs). Insects flap their wings with large wing rotation angles that produce sufficient lift and thrust when flying. The flapping flight mechanisms of insects have drawn much attention for potential applications in MAVs development due to their hovering flight capacity and high maneuverability. Their flapping wings show specific flow structures and their unsteady aerodynamic mechanisms such as leading edge vortex, delayed stall, wake-capture, and rotational circulation in Figure 1. Such criterion has explained how the flapping flights generate lift. Some researchers studied a fundamental approach numerically and experimentally to elucidate aerodynamic force generation in flapping flights. However, most researches used rigid wing models instead of flexible wing models.

The insects have various flexible wing structures, which are very complex to model because their wings are generally made by thin membrane with veins. The majority of prior investigations simplified the wing structural models to assess the benefit of wing flexibilities in force generation due to the complexity on the nonlinear fluid flow. According to previous studies, wings with a specific stiffness could

generate mean lift coefficient similar to that of a rigid wing. However, the appropriate wing flexibility for insect-inspired flapping MAVs and the difference of flow structures between the rigid and flexible wings that affects the aerodynamic forces deterioration have yet to be elucidated.

To solve above questions, this paper describes the experimental setup, including force measurements and digital particle image velocimetry (DPIV) measurements, to study on flapping wing flexibility. Hovering hawkmoth-like wings, derived from *Manduca sexta*, are selected as wing models in preliminary experiment. The wing thickness is chosen as design variables to simplify the comparison between various wing flexibilities. The wing models with spanwise length of 200 mm and an aspect ratio of 6.18, are constrained to a simple harmonic flapping motion with sweeping and rotating angles of  $120^\circ$  and  $90^\circ$  at Reynolds number (Re) of 10,817.

## 2 EXPERIMENTAL SETUP AND PROCEDURE

Figure 1 shows the 3-D flapping motion model in the current study, and wing models are constrained to motion kinematics for hovering flight in water tank with size of  $3.5 \text{ m} \times 1.0 \text{ m} \times 1.1 \text{ m}$ . The motion model for sweeping and rotating the wing is composed of two servo motors as shown in Figure 2. The

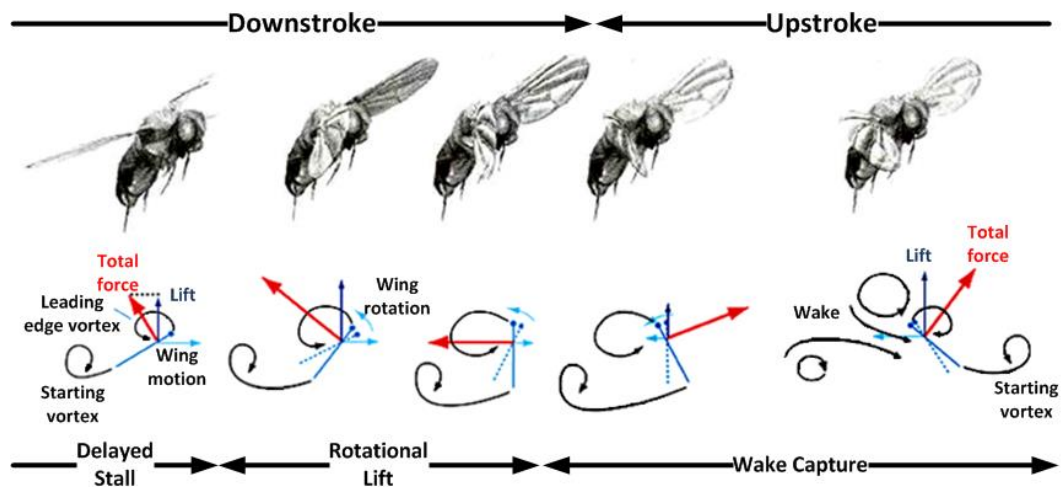


Figure 1 Summary of aerodynamic mechanisms in insect flapping flight, designed by Dickinson, M. H. in "Catching the Wake", SCIENTIFIC AMERICAN™

upper servo motor with a horn, mounted under the upper plate, drives the sweeping motion (stroke angle,  $\phi$ ) along the X-Y plane. The rotation motion (angle of attack,  $\alpha$ ) along the X-Z plane is operated by the lower servo motor.

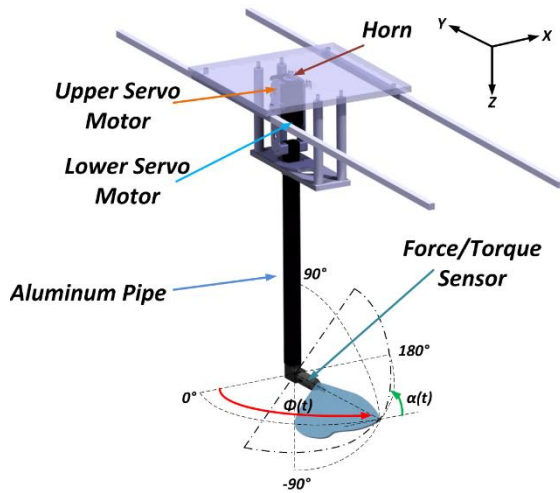


Figure 2 Experimental Motion Model and Motion Coordinates

The hawkmoth-like wing has been used for several years to study insect-inspired flapping MAVs due to its hovering and forward-flight capacities as well as its heavy weight relative to other insects. The geometry of the target model in Figure 3 is borrowed from Usherwood and Ellington (2002). The wing models have a half-span length,  $R$ , of 200 mm, a mean chord length,  $\bar{c}$ , of 64.7 mm, and an Aspect Ratio,  $AR$ , of 6.187. Due to the experimental environment corresponding to the environment of hawkmoth in nature, the wing-beat frequency is much lower than that of the real hawkmoth in nature to maintain the range of Reynolds numbers. In addition, the wing models are made of Polycarbonate (PC) sheet, and the wing thickness is a design variable in the present study. There are eight cases in which there are rigid wing (3 mm-thick) and flexible wings (2, 1, 0.8, 0.5, 0.35, 0.2 and 0.1 mm-thick) as shown in Table 1.

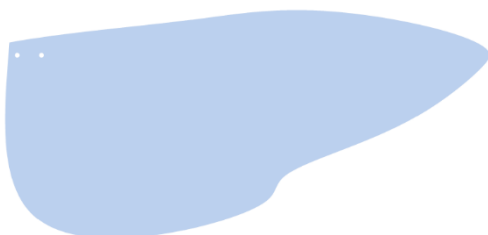


Figure 3 Hawkmoth-like wing model in the present study

Table 1 Wing data in the present experiment

Case	Thickness (mm)	$EI_{non}$
1	3	1892.095
2	2	560.994
3	1	70.124
4	0.8	35.876
5	0.5	8.759
6	0.35	3.005
7	0.2	0.5607
8	0.1	0.07009

Sun and Tang (2002) compared their calculated results in hovering flight with previous data from Ellington (1984), and suggested that a duration of wing rotation ( $t/T_\phi$  and  $t/T_\alpha$ , non-dimensional rotation time along  $\phi$  and  $\alpha$  respectively) was able to assume reasonably 20% of period of one flapping cycle. This motion is considered in this experiment as a symmetrical flapping motion in Figure 4.

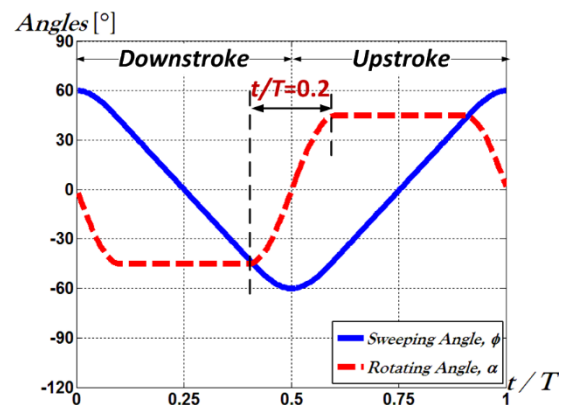


Figure 4 Symmetrical flapping motion

### 3 RESULTS AND DISCUSSION

Figure 5 shows the distributions of lift and drag coefficients from case 1 to 8 in the symmetrical flapping motion. First, the rigid wing (blue, thin solid-line) presents three peaks in the lift coefficient and two peaks in the drag coefficient. The lift coefficient shows dual peaks after the wing reversal and last peak before the wing reversal. The dual peaks can be explained by the wing-wake interaction with the generation of leading edge vortex, and last peak can be explained by the pitching-up motion (rotational force). In the drag coefficient, two peaks after and before the wing reversal are observed. The first peak is caused by the wing

velocity increase with high angle of attack and the wing-wake interaction, and the second peak also occurs due to the pitching-up motion.

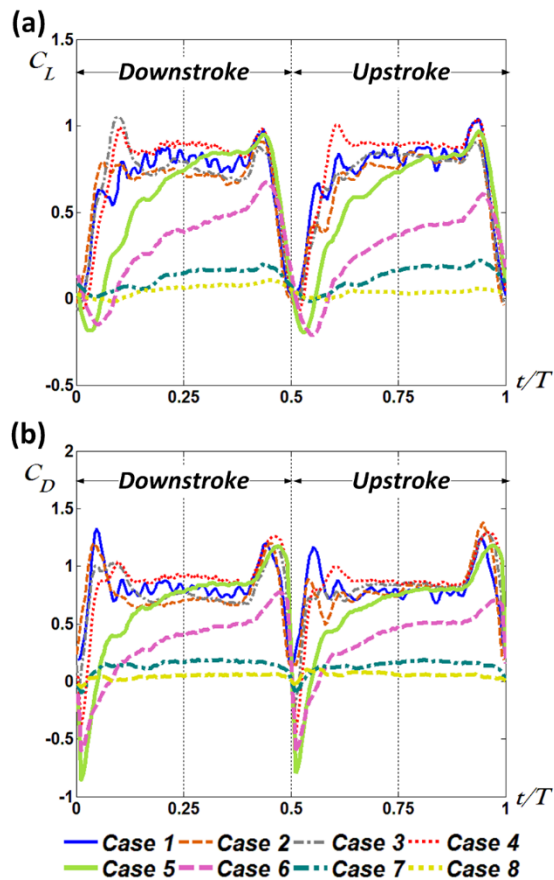


Figure 5 Lift and drag coefficients from case 1 to 8

In the flexible wings, case 1 to 4 show that the first steep peak in the lift increases and one in the drag coefficient decreases as the wing becomes flexible. Case 5 to 8 present that the generation of aerodynamic force is delayed and the magnitude of aerodynamic force decreases as the wing is more flexible. Based on above results, this paper focuses on only four cases, case 1, 4, 5, and 6, with the DPIV results. The reason why this paper selected such cases has demonstrated in the paper in detail.

The symmetrical flapping motion has no significant difference in the vortex structures between the downstroke and upstroke although the lift and drag coefficients each stroke are slightly different. DPIV tests take the images at same chordwise cross-section of  $0.5R$  as the rigid wing. In addition, four capture points are chosen for DPIV tests each stroke:  $t/T = 0.05, 0.1, 0.25,$  and  $0.45$  for downstroke, but this summary shows two captured time,  $t/T = 0.05$  and  $0.1$ , in each case. Figure 6 illustrates the

time-resolved DPIV results to describe the velocity vector field and the vorticity distribution at  $0.5R$  chordwise cross-section in the symmetrical flapping motion.

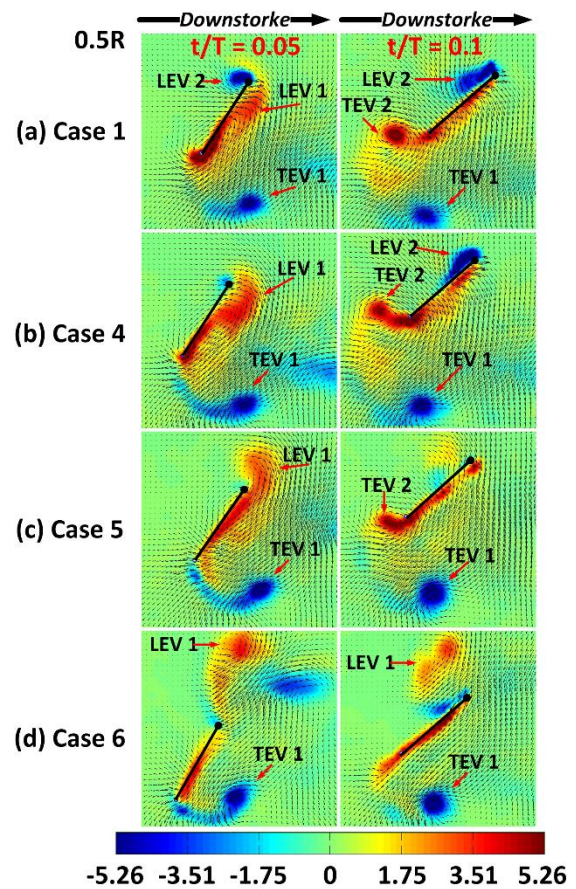


Figure 6 Time-resolved flow structures at  $0.5R$  chordwise cross-section in a symmetrical flapping motion: (a) at  $t/T = 0.05$  and  $0.1$

The important point in the symmetrical flapping motion is the wing-wake interaction after the wing reversal. In the rigid wing (case 1), LEV 1 generated by previous stroke is attached under the wing in the new stroke and TEV 1 is generated close to the wing during reversing the wing. The attached LEV 1 and the TEV 1 indicates that the wake between the vortices induces the flow velocity increase toward the wing. This induced velocity increase with LEV 2 generation causes the lift augmentation right after the wing reversal. In flexible wings, case 4 shows the wing-wake interaction even if the time of its occurrence is a little late than case 1. The time in the wing reversal is delayed due to the delayed-motion of the flexible wing, and especially the hind wing is reversed later than the fore wing. The delayed hind wing generates TEV 1 late, so the

influence of the wing-wake interaction in case 4 arises later than case 1.

Case 5 and 6 show different flow structures during the wing reversal in comparison with previous cases. Figure 6 (c) and (d) describe that LEV 1 disperses above the leading edge, not going down under the wing. The wings with high flexibility are elevated higher than case 1 and 4 for flapping. As replaying the sequential images in case 5 and 6, the wings are going down suddenly for the wing reversal so they generate vortices on high. Therefore, LEV 1 is located above the wing after the wing reversal and the wing loses the effect of the wing-wake interaction to cause the steep increase. In addition, the wing in case 6 generates LEV 2 too late due to the delayed-motion with the distribution of LEV 1 on the wing. The delay in the LEV 2 generation and the small size of the LEV 2 also cause the low lift in case 5 and 6. Consequently, the wing-wake interaction is not acted without LEV 1 even if all cases generate TEV 1 for the wing reversal.

#### 4 CONCLUSION

This study has investigated the effects of flapping hawkmoth-like wing flexibility on the aerodynamic characteristics in a symmetrical flapping motion. The aerodynamic force generally decreases as the wing become flexible, but case 4 (0.8 mm-thick) has more aerodynamic force than rigid and other flexible wings. Moreover, the lift and drag coefficients of case 5 to 8 (0.5, 0.35, 0.2, and 0.1 mm-thick) decrease extremely as the wing becomes thinner. These findings present that the flexible wings have effects on the improvement of aerodynamic force as well as on the decline of

aerodynamic force. They also demonstrate that the wings with high flexibility as well as the rigid wing are unsuitable for flapping flight in MAVs.

Furthermore, the power required is an important factor to maintain the steady level flight in propulsion system. MAVs are very small and have low velocity so they need the efficient power consumption to obtain the aerodynamic force over their weight. When  $C_L^{1.5}/C_D$  is a maximum value, the minimum power required occurs. Figure 7 shows  $C_L^{1.5}/C_D$  from case 1 to 8 in the symmetrical flapping motion. This experiment has the highest  $C_L^{1.5}/C_D$  in case 4, and it shows that case 5 has similar value to case 1 and 3 so the flexible wings in case 5 is efficient enough to generate the aerodynamic force compared to the rigid wing (case 1). These results describe that the specific flexibility is an important point for the development of the insect-inspired flapping MAVs with the flapping kinematics.

These findings demonstrate the importance to study the flexible flapping wing in hovering flight, and they can motivate the researchers to look forward the range of the specific flexural stiffness for the development of Insect-inspired flapping MAVs with better aerodynamic efficiency. However, this finding is still difficult to find the specific flexibility with high aerodynamic efficiency in hovering flight. Because the flow structures are influenced by both flapping kinematics and wing flexibility, it is not easier that some specific range of flexibility is better to design the insect-inspired flapping MAVs. In future, it is implemented for above flexible wings to ever obtain the high aerodynamic efficiency in the similar kinematics to real hawkmoth flight.

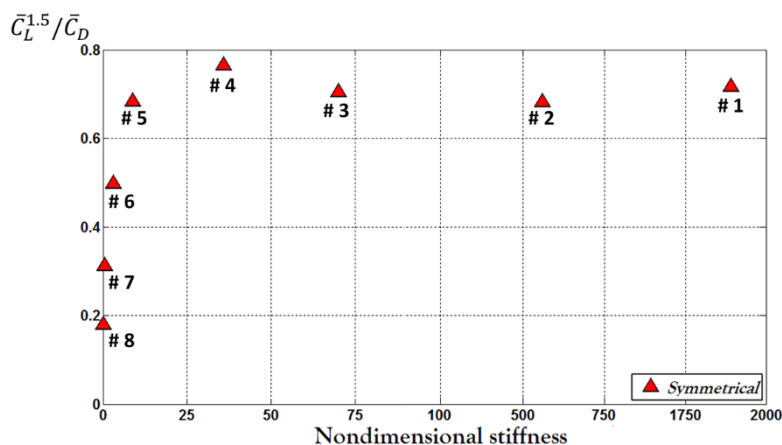


Figure 7  $C_L^{1.5}/C_D$ , from case 1 to 8, in symmetrical flapping motion